ISBN: 978-3-95450-225-7 ISSN: 2673-5571 doi:10.18429/JACoW-HB2021-MOP19

OPTIMISED TRANSVERSE PAINTING SCHEMES FOR THE NEW 160 MeV H⁻ INJECTION SYSTEM AT CERN

E. Renner*[1], S. Albright, F. Antoniou, F. Asvesta, H. Bartosik,
C. Bracco, G. P. Di Giovanni, B. Mikulec, T. Prebibaj[2],
F. M. Velotti, CERN, Geneva, Switzerland
[1]also at TU Wien, Vienna, Austria
[2]also at Goethe University, Frankfurt, Germany

Abstract

A major aspect of the LHC Injectors Upgrade (LIU) project at CERN is the Proton Synchrotron Booster (PSB) connection to the newly built Linac4 and the related installation of a new 160 MeV H⁻ charge exchange injection. This contribution presents the first operational experience with the new injection system and its flexibility of applying horizontal phase space painting to tailor different beams to the respective user-defined brightness targets. The presented measurement and multi-particle simulation results focus on the optimisation of the required transverse injection settings to reduce losses when producing high-intensity beams, i.e. for the ISOLDE experiment. In this context, feasibility studies towards applying numerical optimisation algorithms for improving and efficiently adapting the respective injection settings online are presented.

INTRODUCTION

The PSB is the first synchrotron in the CERN injector complex and consists of four superposed rings. It was upgraded during the Long Shutdown 2 (LS2) in 2019/2020 as part of the LIU project [1], with the aim of doubling the beam brightness for the High Luminosity LHC [2] era. When connecting the new 160 MeV H⁻ accelerator Linac4 [3] to the PSB, the injection energy was increased from 50 to 160 MeV and with it the relativistic factor $\beta_r\gamma_r^2$ by a factor two. A key component of this connection is the newly installed charge exchange injection system [4], which replaces a conventional proton multi-turn injection. The injection process into the PSB is used for tailoring the wide range of transverse beam characteristics as requested by the various users at CERN, covering intensities from $N_{p_+} = \mathcal{O}(10^{10})$ to $\mathcal{O}(10^{13})$ protons per ring and normalized transverse emittances from $\epsilon_{n,\mathrm{rms}}$ <0.7 µm (LHC-like beams) to ≈ 9–10 µm (high intensity, e.g. for the ISOLDE [5] or nTOF [6] experiment). Prior to the upgrade, the production of the high intensity fixed target beams with $N_{p_+} = 0.8 - 1 \cdot 10^{13}$ p+ per ring resulted in up to 30 − 40% losses at the injection septum due to the nature of the conventional multi-turn injection. With the new injection system, similar beams can be produced while keeping the losses within a few percent.

The required transverse beam characteristics for each user are customized by defining the programmable field decay of the horizontal injection bump as well as the offset between injected beam and circulating beam orbit during the injection process. This tailoring of the phase space distribution during injection is referred to as phase-space painting and enables a reduction of the charge density during beam accumulation, particularly when injecting high intensity beams. Consequently, the space charge detuning is reduced and emittance growth due to interaction of the detuned protons with integer resonances mitigated. Adequate painting schemes to produce operational beams with the same parameters as before the upgrade (pre-LS2) were previously defined using multi-particle simulations [1, 7–9]. These have been refined with beam and are now successfully used in operation. However, automatically optimising these programmed transverse painting schemes based on pulse per pulse modulation user requests and beam instrumentation feedback becomes a key aspect to improve operational efficiency, especially considering the perspective of increasing the delivered intensity for selected fixed target beams to $I > 1 \cdot 10^{13}$ p+ per ring.

This contribution presents simulation and measurement results to assess the impact of applied transverse painting settings on the losses obtained during high intensity beam production, taking an ISOLDE-like beam as an example. Subsequently, we discuss the potential of applying numerical optimisation algorithms to set and adapt the transverse painting functions automatically.

PSB CHARGE EXCHANGE INJECTION AND PAINTING SETTINGS

The Linac4 H⁻ beam features normalised transverse emittances $\epsilon_{u,n}$ ≈0.3 µm in both planes $u = x, y$. Beam can be accumulated in the PSB over up to $n_t = 150$ turns, which corresponds to an injection over $t_{\mathrm{INJ}} = 150$ µs considering the PSB revolution period at injection energy $\tau \approx 1$ µs. For the here presented high intensity beam production studies, a chopping factor of $CF = 0.6$ is applied to the H⁻ beam. This results in an injected intensity of $I_{\mathrm{INJ/turn}} \approx 1 \cdot 10^{11}$ p+ per PSB turn of beam accumulation [9], based on the present Linac4 peak current of 26 mA. The PSB accelerates beam from 160 MeV to 2 GeV in 530 ms with a 1.2 s repetition rate. In this contribution, we use time in ms relative to the start of the cycle ("C-time") to refer to time instances. Injection takes place at C275, extraction at C805.

The new injection system is illustrated in Fig. 1. The H⁻ beam coming from Linac4 (red in Fig. 1) is injected via a ≈200 µg cm^{-2} carbon stripping foil [10–13]. The already circulating beam (blue in Fig. 1) is horizontally deflected towards the foil by a chicane in the injection region [14],

* elisabeth.renner@cern.ch

ISBN: 978-3-95450-225-7 ISSN: 2673-5571 doi:10.18429/JACoW-HB2021-MOP19

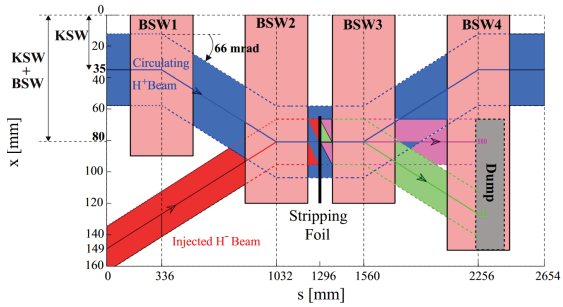

Figure 1: Schematic of the PSB H^- injection system (KSW: painting kicker magnets, BSW: injection chicane) [1].

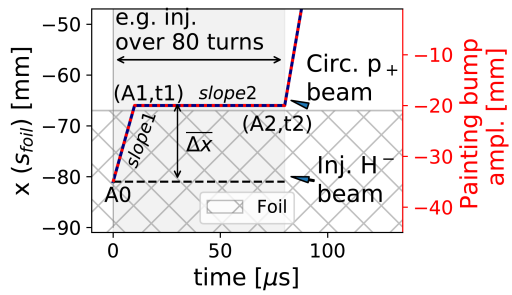

Figure 2: Circulating orbit at the stripping foil during the painting bump decay. Left axis: combined deflection of chicane and painting bump, right: painting bump amplitude.

creating a bump of −46 mm amplitude, and by painting kickers with nominal bump amplitude of −35 mm and variable field decay [15, 16]. The painting kicker field modulation during injection is controlled by piece-wise linear functions. Figure 2 illustrates the time evolution of the closed orbit at the location of the stripping foil, when applying a painting kicker field decay as programmed for example for high intensity beams. The nominal position of the injected beam (−81 mm) is indicated for reference by the dashed line. The maximum bump amplitude A_0 defines the offset of the circulating orbit with respect to the injected beam when injecting the first bunch. The horizontal phase space distribution and the resulting painted beam size is mainly tailored by setting slope 1, which is defined by the amplitude-marker pair A_1 and t_1. Slope 2 (A_2, t_2) controls the subsequent intensity accumulation. t_2 [μs] marks the end of the injection process and is set equal to number of PSB revolutions during beam accumulation. The vertical beam size can be tailored by applying a fixed vertical offset Δy [mm] or angle $\Delta y'$ [mrad] to the injected beam using corrector magnets in the injection line. However, as there is no difference expected between applying an offset or angle, we consider for the following report only the impact of optimising Δy while setting $\Delta y' = 0$ mrad.

PHASE SPACE PAINTING FOR HIGH INTENSITY FIXED TARGET BEAMS

In this section, injection painting studies for an ISOLDE-like beam are presented with machine configurations as summarised in Table 1. It has to be noted that machine optimisation studies, including resonance compensation and working point optimisations [17], are ongoing. The working conditions presented here are used to commission the transverse painting logic for high intensity beams and develop tools for optimisation, which can be transferable to future machine configurations, as described below.

Table 1: Parameters for Painting Studies on ISOLDE Beams

	Parameter	Unit	Measurement Config.
General	Ring		3
	I_{INJ} / n_t	p+ /	$805 \cdot 10^{10}$ / 80
	$dE_{rms,\mathrm{INJ}}$	keV	280
	Q_x / Q_y		4.22 / 4.36
Painting	t_1, t_2	μs	10, 80
	A_0	mm	-35
	A_1	mm	-26 (-29 to -20)
	A_2	mm	as A1
	Δy	mm	0 (0-6)
Results	$\epsilon_{n,y,\mathrm{RMS}}$ / $\epsilon_{n,y,\mathrm{fit}}$	μm	≈ 5 – 5.5 / ≈ 6
	$\epsilon_{n,x,\mathrm{RMS}}$ / $\epsilon_{n,x,\mathrm{fit}}$	μm	≈ 7.5 – 10.5 / ≈ 9 – 14
	L_{C805}	%	2.6 (2.6-7.5)

Motivation and Constraints

For ISOLDE beams, injection setting optimisation is intended to reduce the losses along the cycle and maximise the beam transfer, not to tailor a specific beam size. Limitations for the extent of the painted transverse emittances of ISOLDE beams are only given by the minimum PSB acceptance. Previous studies estimate maximum allowed normalised 1σ emittances of $\epsilon_{n,x,\max} = 9$ mm mrad [18] and $\epsilon_{n,y,\max} = 6$ mm mrad [19] in order to fit the beam into the horizontal $4\sigma_{x,\max}$ and vertical $2.5\sigma_{y,\max}$ acceptance (recombination part of the extraction line), respectively. A new absorber system comprising a movable and a fixed mask was installed during LS2 to protect those identified bottlenecks [20]. During the here presented measurement campaign, the PSB was operated without the movable mask inserted. The resulting aperture bottleneck generated by the fixed mask features per design an acceptance of $4\sigma_{x,\max}$ and $3.5\sigma_{y,\max}$, assuming a Gaussian transverse distribution [20]. However, it has to be noted that the obtained profiles generally feature strongly under-populated tails and that acceptance limitations are not the dominant cause of losses.

Simulation and Measurement Set-Up

For this first assessment of different injection painting settings we keep t_1, A_0 and t_2 constant. Vertically, the offset of the injected beam is varied $\Delta y = 0 - 6$ mm. Horizontally we set $A_1 = A2 = -29$ to -20 mm, resulting in a variation of the effective offset between injected beam position and circulating beam orbit during beam accumulation of $\Delta\bar{x} = 6 - 15$ mm (Fig. 2). As in the previous studies presented in [10], the probed configurations span both extremes: Transverse injection settings resulting in controlled transverse emittance blow up dominated by the applied paint-

ISBN: 978-3-95450-225-7 ISSN: 2673-5571 doi:10.18429/JACoW-HB2021-MOP19

ing ($\Delta y = 6$ mm and $\Delta\bar{x} = 12 - 15$ mm), and uncontrolled emittance growth due to increased space charge detuning and interaction of the beam core with integer resonances ($\Delta y = 0 - 3$ mm and $\Delta\bar{x} = 6$ mm).

The obtained losses throughout the cycle are defined as

$$L_{\mathrm{C805}} = \frac{|I_{\mathrm{BI,INJ}}| - I_{\mathrm{BR,EXTR}}}{|I_{\mathrm{BI,INJ}}|} \quad (1)$$

where $|I_{\mathrm{BI,INJ}}|$ is the intensity of the H^- beam measured in the injection line and $I_{\mathrm{BR,EXTR}}$ the intensity observed with the ring beam current monitor immediately before extraction (C805). Additional losses in the extraction line are not considered in this work. All presented wire-scans are taken at extraction energy close to the end of the cycle (C770) using the newly installed LIU wirescanners [21]. Measurement of the longitudinal profile and a tomographic reconstruction [22] are used to calculate the momentum spread at extraction time, which was $\frac{dp}{p} \approx 1.1 \pm 0.06 \cdot 10^{-3}$.

Comparative multi-particle simulations of the injection process are conducted for the first 5 ms, i.e. up to C280, using PTC-pyOrbit [23]. Foil scattering, optics perturbation due to the injection chicane [24] and a quadrupolar error are included in the simulations.

Observations in Simulations and Measurements

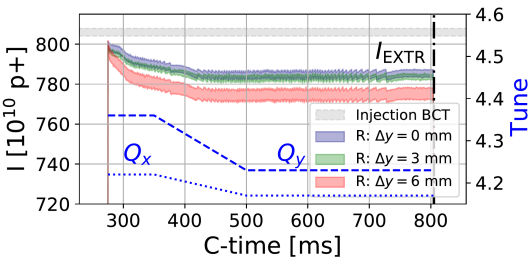

Figure 3: Measured intensity along the cycle (1σ errorbar, injection: C275, extraction: C805) for $\Delta\bar{x} = 9$ mm and different vertical offsets, compared to the intensity measured in the injection line (grey). The programmed tune evolution (blue) is displayed using the second axis.

Figure 3 displays the characteristic of the measured current along the cycle for a subset of the probed settings. Losses during the injection process itself (C275) mainly due to beam size limitations account for $L_{\mathrm{C275}} \approx 0.6 - 1 \pm 0.1$ %. For the applied settings the majority of the losses are observed up to C450 due to interaction with various resonances [17, 25]. The dependence of the total obtained losses on the probed injection settings is summarised in Fig. 4. For $\Delta\bar{x} = 6$ mm (space charge dominated blow-up of ϵ_x), the losses decrease when applying a vertical offset $\Delta y > 0$ mm. On the other hand, for $\Delta\bar{x} = 9 - 15$ mm (painting dominated blow-up of ϵ_x), the losses increase with increasing Δy. Considering the probed injection settings as displayed in Fig. 4, minimal losses of $L_{805,\,\mathrm{min}} \approx 2.6 \pm 0.2$% are obtained for $\Delta y = 0$ mm and $\Delta\bar{x} = 9$ mm. We note, that this considerable dependence of the obtained losses to the applied Δy

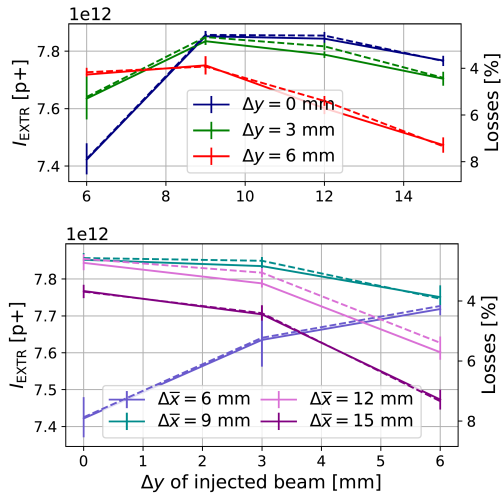

Figure 4: Measured intensity before extraction (solid) for different painting settings. The corresponding losses with respect to the injected intensity are displayed using the second axis (dashed).

is observed despite the resulting vertical emittances being similar in all cases, as illustrated in Fig. 5 (centre and right).

Figure 5 (left) shows the tune footprints as obtained in simulations after 5 ms, i.e. at C280. For cases with increased losses, the footprints show a shift of the vertical tune distribution's peak towards increased Q_y (blue in Fig. 5a and red in Fig. 5c), indicating an enhanced probability to excitation due to resonance crossing. The vertical profiles measured at C770 are presented in Fig. 5 (centre). The profiles are compared to a Gaussian distribution $\mathcal{N}\left(\sigma_y\left(\epsilon_{n,y} = 6\ \mu\mathrm{m}\right)\right)$ as this corresponds to the beam size assumed for the aperture limitation described above. The residuals of the obtained distributions with respect to $\mathcal{N}\left(\sigma_y\left(\epsilon_{n,y} = 6\ \mu\mathrm{m}\right)\right)$ are plotted in Fig. 5 to illustrate the difference in tail population. The presented profiles feature an increased vertical tail population for painting settings with increased losses, mainly visible for $\Delta\bar{x} = 6$ and 15 mm. However, these results have to be considered with care, as acquired profiles, and particularly the tails, are distorted by the wire-scanner acquisition [26]. As the wire crosses the beam in Fig. 5 from left to right, the left side of the profile ($y = -10$ to -5 mm) is considered less affected by such scattering distortions.

The presented measurements give first indications towards the optimised injection settings. For the present operational configuration we summarise that it is not beneficial to paint a large transverse emittance at injection in both planes, as the reduced initial tune spread both, horizontally and vertically, results in increased losses during resonance crossing. To profit from the complete painting kicker's flexibility, A_0, t_1 and t_2 can additionally be varied to obtain minimised losses. Further, the applied painting function may need to be adapted when changing the operating conditions such as injected intensity, working point, energy spread or resonance compensation. This sensitivity of the optimum injection settings to varying operational conditions makes automatic tuning of injection settings attractive, as discussed below.

ISBN: 978-3-95450-225-7 ISSN: 2673-5571 doi:10.18429/JACoW-HB2021-MOP19

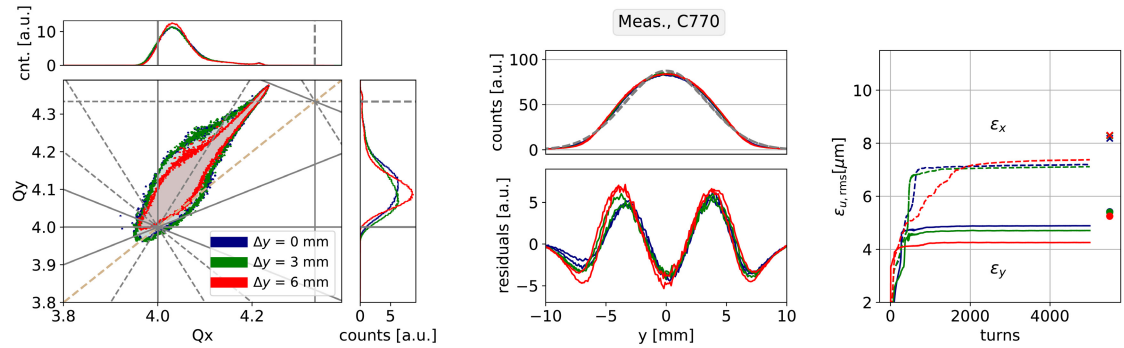

(a) $\Delta\bar{x}$ = 6 mm

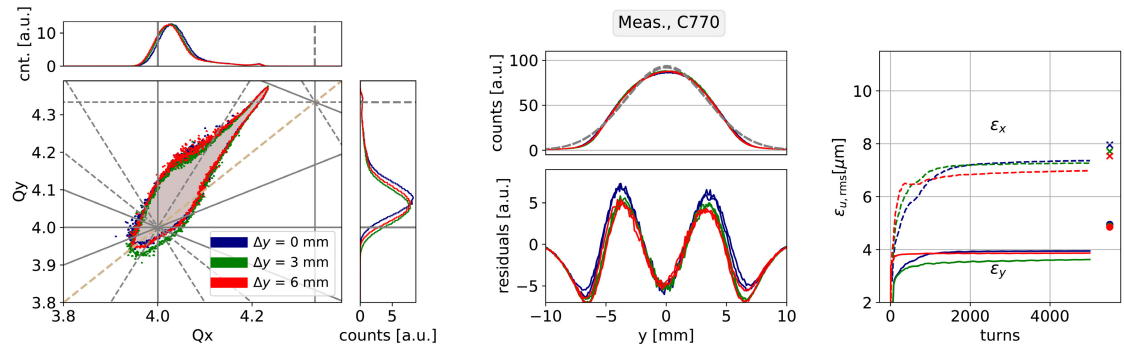

(b) $\Delta\bar{x}$ = 9 mm

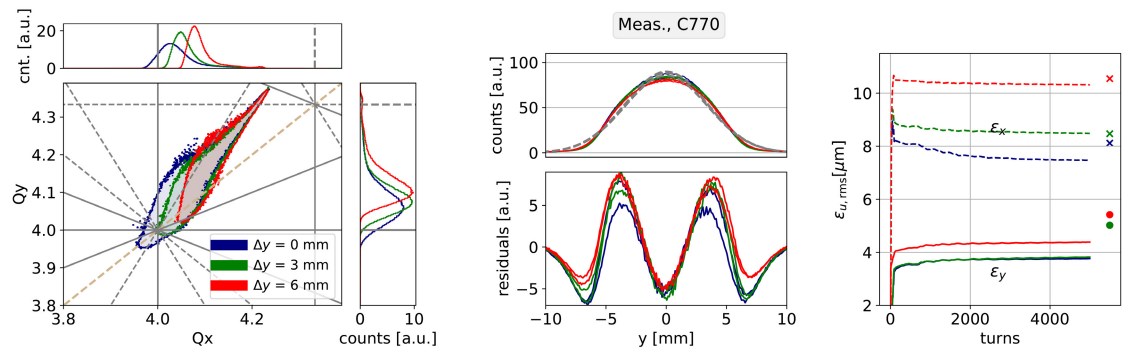

(c) $\Delta\bar{x}$ = 15 mm

Figure 5: Simulation and measurement results for various painting settings. Left: Tune footprints for C280 obtained from multi-particle simulations for different painting scenarios. Centre: Measured vertical profiles (at C770) for different injection painting scenarios, compared to a Gaussian distribution for ϵ_y = 6 µm (grey dashed). Right: Simulated intensity and r.m.s.-emittance evolution up to C280. $\epsilon_{u,\mathrm{rms}}$ measured at C770 are displayed with cross (x) and circle (y) markers.

TOWARDS APPLYING NUMERICAL OPTIMISATION ALGORITHMS

Numerical optimisation algorithms are increasingly employed within the CERN accelerator complex to enhance operational and commissioning efficiency. During beam commissioning, tools to optimise the transverse injection settings for various users are being developed and probed using the in-house Generic Optimisation Frontend and Framework (GeOFF) [27]. For the above described ISOLDE beams, the optimisation environment allows variation of 5 parameters, A_0, t_1, A_1, v_2 $(t_2, A_2) = \frac{dx}{dt}$ of slope 2 and Δy. We optimise on a loss function as defined in Eq. (1). If required, the loss function can be expanded by including various intensity and loss measurements in the injection, extraction region and the ring to weight location and temporal occurrence of losses.

Different derivative-free numerical optimisation algorithms have been considered for this problem, i.e. pyBOBYQA [28, 29], Powell [30], COBYLA [31] and Nelder-Mead [32]. Whereas the latter did not converge to a solution within ≈ 100 steps, we obtain a reasonable performance of pyBOBYQA, COBYLA and Powell for the first optimisation attempts, which converge to acceptable solutions within 30–100 steps. To state an example, the progress of an optimisation run using pyBOBYQA is displayed in Fig. 6 (left). Data acquired for a fixed machine configuration (ring 3, $|I_{\mathrm{BI,INJ}}| \approx 0.9 \cdot 10^{13}$ p+) over multiple optimisation runs with different algorithms and hyper-parameter settings is used

ISBN: 978-3-95450-225-7 ISSN: 2673-5571 doi:10.18429/JACoW-HB2021-MOP19

for analysis of the feature space. The minimum loss surface for selected feature combinations highlights the convex characteristic and the flat minimum of the problem (centre and right in Fig. 6). The steps taken by the optimisation algorithm in this exemplary run are indicated by scatter markers. For this dataset (acquired over multiple opimisation runs), the probed painting bump decays and applied vertical offsets are displayed in Fig. 7, color-coded by the losses obtained when applying the respective settings.

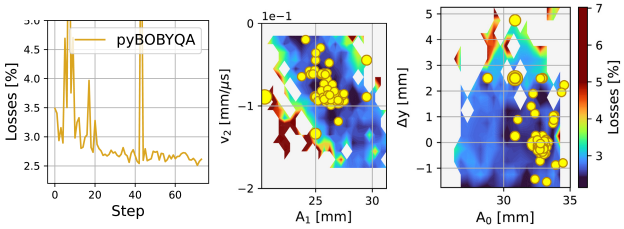

Figure 6: Example for optimisation progress using pyBOBYQA (left) and illustration of optimisation steps in selected feature subspaces (centre, right).

To compare the solutions obtained for different machine configurations (rings, intensities), the settings resulting in minimal losses (blue in Fig. 7) are selected for each scenario and corresponding parameter spans illustrated in Fig. 8. As expected, the optimised loss levels differ for the various operational conditions, for example 2.3% in ring 3 compared to 4% in ring 2 for $|I_{\mathrm{BI,INJ}}| \approx 0.9 \cdot 10^{13}$ p+. Still, the characteristic of the optimised injection configurations stays similar. As in the study presented above, the optimised settings converge to $\Delta y \approx 0$ mm. The horizontal painting converges towards solutions with an amplitude decay $|A_2| < |A_1|$, compared to the studies presented above in which we chose $|A_2| = |A_1|$. However, considering the flat minimum (Fig. 6), a dependency of this obtained horizontal painting bump decay on the initial conditions has not been excluded so far.

Detailed studies to assess the optimised injection configurations as well as to improve the optimiser performance are ongoing. A surrogate model is trained with a Random Forest Regressor [33] using the presented dataset acquired during the first optimisation runs. This model is used for ongoing studies regarding offline hyper-parameter and loss-function tuning as well as algorithm performance evaluation. The high noise level of the loss function ($\sigma_{\mathrm{noise}} = 6\%$ of the objective value) as well as the flat minimum prove to be some of the major challenges. Further, keeping the aim in mind to operationally use this tool to efficiently adapt to new operational conditions, the focus when tuning the hyper-parameters is put on providing a high sample efficiency.

SUMMARY

The new PSB H^- injection enables tailoring of the transverse phase space distribution during injection. The impact of transverse painting schemes on losses during high intensity beam production has been assessed with beam and compared to multi-particle simulations. We observe a significant

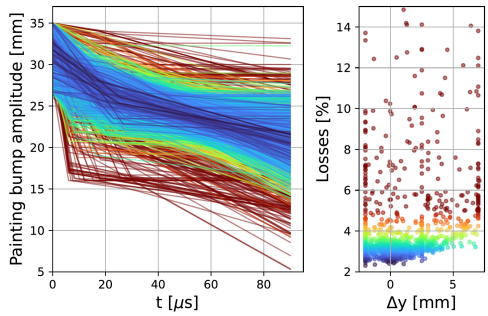

Figure 7: Selection of injection settings obtained in optimiser steps: Horiz. painting bump decay during beam accumulation (left), applied Δy of injected beam (right). Data collected over multiple runs for $I_{\mathrm{INJ}} = 0.9 \cdot 10^{13}$p+, R3.

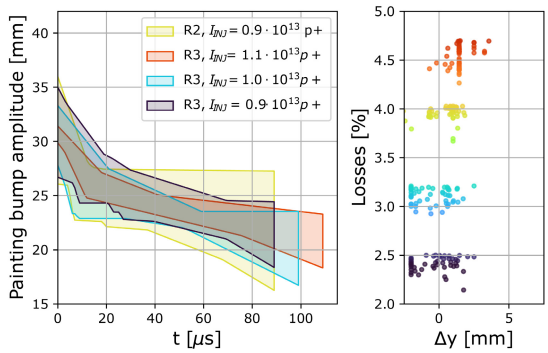

Figure 8: Comparison of the injection settings range as optimised by using diverse numerical optimisation algorithms for different operational conditions.

dependency of the vertical losses obtained during resonance crossing to the applied transverse painting settings and the resulting phase space distribution after injection. Promising results have been obtained when applying numerical optimisation algorithms to efficiently optimise the transverse injection settings to reduce those losses during high intensity beam production. A data driven surrogate model is being used for offline hyper-parameter tuning and feature engineering to improve the optimisation set-up.

ACKNOWLEDGMENTS

The authors would like to thank all teams involved in the PSB and Linac4 operation, hardware and beam commissioning for their continuous support and input, as well as V. Kain and N. Madysa for development of and support with the Generic Optimisation Frontend and Framework.

REFERENCES

[1] J. Coupard *et al.*, "LHC Injectors Upgrade, Technical Design Report, Vol. I: Protons", CERN, Geneva, Switzerland, Rep. CERN-ACC-2014-0337. 2014.

[2] G. Apollinari, *et al.*, "High-Luminocity Large Hadron Collider (HL-LHC): Technical Design Report V. 0.1", *CERN-2017-007-M*, CERN, Geneva, 2017. doi:10.23731/CYRM-2017-004

ISBN: 978-3-95450-225-7 ISSN: 2673-5571 doi:10.18429/JACoW-HB2021-MOP19

[3] L. Arnaudon *et al.*, "Linac4 Technical Design Report", CERN, Geneva, Switzerland, Rep. CERN-AB-2006-084, 2006.

[4] W. J. M. Weterings *et al.*, "The New Injection Region of the CERN PS Booster", in *Proc. IPAC'19*, Melbourne, Australia, May 2019, pp. 2414–2417. doi:10.18429/JACoW-IPAC2019-WEPMP039

[5] B. Jonson and K. Riisager, "The ISOLDE facility", *Scholarpedia*, vol. 5(7), p. 9742, 2010. doi:10.4249/scholarpedia.9742

[6] A. Mengoni *et al.*, "Status and perspectives of the neutron time-of-flight facility nTOF at CERN", in *EPJ Web Conf. 239*, 2020. doi:10.1051/epjconf/202023917001

[7] E. Renner *et al.*, "PSB simulation studies for post LS2 operation", presented at *4th ICFA Mini-Workshop on Space Charge*, CERN, Geneva, Switzerland, Nov. 2019.

[8] V. Forte, "Performance of the CERN PSB at 160 MeV with H^- charge exchange injection, CERN, Geneva, Switzerland, Rep. CERN-THESIS-2016-063, Jun. 2016.

[9] V. Forte *et al.*, "Multi-Particle Simulations of the Future CERN PSB Injection Process with Updated Linac4 Beam Performance", in *Proc. HB'19*, Daejeon, Korea, Jun. 2018, pp. 278–283. doi:10.18429/JACoW-HB2018-WEP2PO007

[10] E. Renner *et al.*, "Beam Commissioning of the New 160 MeV H^- Injection System of the CERN PS Booster", in *Proc. IPAC'21*, Campinas, SP, Brazil, May 2021, pp. 3116–3119. doi:10.18429/JACoW-IPAC2021-WEPAB210

[11] B. Goddard *et al.*, "Stripping Foil Issues for H- Injection into the CERN PSB at 160 MeV", in *Proc. IPAC'10*, Kyoto, Japan, May 2010, paper THPEB030, pp. 3951–3953.

[12] C. Bracco *et al.*, "Commissioning of the Stripping Foil Units for the Upgrade of the PSB H- Injection System", in *Proc. IPAC'17*, Copenhagen, Denmark, May 2017, pp. 595–598. doi:10.18429/JACoW-IPAC2017-MOPIK041

[13] C. Bracco *et al.*, "Measurements with the stripping foil test stand in the Linac4 Transfer Line", in *Proc. INTDS'18*, East Lansing, United States, Oct. 2018, p. 01003. doi:10.1051/epjconf/202022901003

[14] B. Balhan *et al.*, "Design and Construction of the CERN PS Booster Charge Exchange Injection Chicane Bumpers", in *Proc. IPAC'18*, Vancouver, Canada, Apr.-May 2018, pp. 2575–2577. doi:10.18429/JACoW-IPAC2018-WEPMF082

[15] L. M. C. Feliciano *et al.*, "A New Hardware Design for PSB Kicker Magnets (KSW) for the 35 mm Transverse Painting in the Horizontal Plane", in *Proc. IPAC'15*, Richmond, VA, USA, May 2015, pp. 3890–3892. doi:10.18429/JACoW-IPAC2015-THPF086

[16] G. Gräwer, "A multi-waveform pulsed current generator for slow kicker magnets", in *Proc. EPE'19*,Genova, Italy, September 2-5, 2019. doi:10.23919/EPE.2019.8915536

[17] F. Asvesta *et al.*, "Resonance Compensation for High Intensity and High Brightness Beams in the CERN PSB", presented at HB'21, virtual, paper MOP06, this conference.

[18] C. Bracco *et al.*, "PSB injection beam dynamics", presented at *LIU Day 14*, CERN, Geneva, Switzerland, Apr. 2014. https://indico.cern.ch/event/299470/contributions/686522/

[19] J. Abelleira Fernandez, "Beam Dynamics Study on LIU High Intensity Beams in the BT Line", CERN EDMS 1537199 v.1.0, CERN, Geneva, Switzerland, Nov. 2015. https://edms.cern.ch/document/1537199/1.0

[20] H. Bartosik, G. P. Di Giovanni, B. Mikulec, and F. Schmidt, "PS Booster Beam Absorber/Scraper after LS2", CERN EDMS 1578463 v.2.1, CERN, Geneva, Switzerland, Jan. 2018. https://edms.cern.ch/document/1578463/2.1

[21] R. Veness *et al.*, "Installation and Test of Pre-series Wire Scanners for the LHC Injector Upgrade Project at CERN", in ICCS , Copenhagen, Denmark, May 2017, pp. 412-414. doi:10.18429/JACoW-IPAC2017-MOPAB121

[22] S. Hancock, "A simple algorithm for longitudinal phase space tomography", CERN-PS-RF-NOTE-97-06, CERN, Geneva, May 1997. https://cds.cern.ch/record/1174559/

[23] A. Shishlo *et al.* "The Particle Accelerator Simulation Code PyORBIT", in *Proc. ICCS'15*, Reykjavík, Iceland, Jun. 2015, pp. 1272–1281.

[24] T. Prebibaj *et al.*, "Injection chicane beta-beating correction for enhancing the brightness of the CERN PSB beams", presented at HB'21, virtual, paper MOP18, this conference.

[25] A. Santamaria Garcia *et al.*, "Identification and Compensation of Betatronic Resonances in the Proton Synchrotron Booster at 160 MeV", in *Proc. IPAC'19* , Melbourne, Australia, May 2019, pp. 1054–1057. doi:10.18429/JACoW-IPAC2019-MOPTS086

[26] A. Santamaría García *et al.*, "Systematic Studies of Transverse Emittance Measurements Along the CERN PS Booster Cycle", in *Proc. IPAC'18*, Vancouver, Canada, Apr.-May 2018, pp. 806–809. doi:10.18429/JACoW-IPAC2018-TUPAF047

[27] V. Kain and N. Madysa, "Generic Optimisation Frontend and Framework (GeOFF)", https://gitlab.cern.ch/vkain/acc-app-optimisation/

[28] C. Cartis *et al.*,"Improving the Flexibility and Robustness of Model-Based Derivative-Free Optimization Solvers", *ACM TOMS*, vol. 45, no. 3, p. 32, Aug. 2019. doi:10.1145/3338517

[29] C. Cartis *et al.*,"Escaping local minima with local derivative-free methods: a numerical investigation", *Optimization*, Feb. 2021. doi:10.1080/02331934.2021.1883015

[30] M. J. D. Powell, "An efficient method for finding the minimum of a function of several variables without calculating derivatives", *The Computer Journal*, vol. 7, no. 2, pp. 155–162, 1964. doi:10.1093/comjnl/7.2.155.

[31] M. J. D. Powell, "A direct search optimization method that models the objective and constraint functions by linear interpolation", in *Advances in Optimization and Numerical Analysis*, vol. 275, p. 51-67, Springer, Dodrecht, 1994. doi:10.1007/978-94-015-8330-5_4

[32] John A. Nelder and R. Mead, "A simplex method for function minimization", in *Computer Journal*, vol. 7, no. 4, p. 308–313, 1965. doi:10.1093/comjnl/7.4.308

[33] L. Breiman *et al.*, "Random Forests" *Machine Learning*, vol. 45, p. 5–32, 2001. doi:10.1023/A:1010933404324